The International Journal of Advanced Manufacturing Technology (2025) 136:5625–5639
https://doi.org/10.1007/s00170-025-15130-9

ORIGINAL ARTICLE

Investigation of the mechanical machinability of an interpenetrating metal-ceramic composite using diamond grinding

Achim Rösiger[1] · Joél Schukraft[2] · Ralf Goller[1] · Kay A. Weidenmann[2]

Received: 11 October 2024 / Accepted: 29 January 2025 / Published online: 13 February 2025

Abstract

In this study, the mechanical machinability of an interpenetrating metal-ceramic composite was investigated. The material was manufactured by gas pressure infiltration of a slurry-based ceramic preform and an AlSi10Mg cast alloy. The combination of a soft metal and a very hard ceramic brings many advantages in mechanical performance of the composite but challenges in the mechanical machining. Near net shape components manufactured and finished by mechanical processing is of interest. Therefore, diamond-grinding with different diamond grit tipped tools was investigated in a range of process parameters, such as the rotation speed, feed rate, and cutting depth. During the grinding process, the cutting forces were continuously measured, and the machined surface and tool quality were evaluated afterwards. Cold welding of the aluminum chips on the tool and the material surface were detected, and the effect of the superposition of ductile and brittle cutting mechanisms were observed. Increasing cutting forces and therefore increasing the process heat results in reclosing of brittle defects in Al_2O_3 by deformed aluminum. This effect leads to a reduced surface roughness when increasing the material removal rate by increasing cutting speed, feed rate, and cutting depth.

Keywords Interpenetrating metal-ceramic composites (IMCC) · Mechanical machinability · Grinding · Cutting forces · Surface roughness · Material removal behavior

Abbreviations

MMC	Metal matrix composites
MRR	Material removal rate
IMCC	Interpenetrating metal-ceramic composites
IPC	Interpenetrating phase composites
GRA	Grey relational analysis
CNC	Computer numerical control
WJM	Water jet machining
USM	Ultrasonic machining
EDM	Electrical discharge machining
ECM	Electro-chemical machining

✉ Achim Rösiger
achim.roesiger@tha.de

✉ Joél Schukraft
joel.schukraft@mrm.uni-augsburg.de

[1] Faculty of Mechanical and Process Engineering, Technical University of Applied Sciences Augsburg, An Der Hochschule 1, 86161 Augsburg, Germany

[2] Institute of Materials Resource Management, University of Augsburg, Am Technologiezentrum 8, 86159 Augsburg, Germany

1 Introduction

The consequent development of materials, to improve their structural properties such as stiffness, strength, and wear resistance, brought up various composite materials in the last decades [1]. In particular, the combination of opposing materials has challenged the development of hybrid composites to combine the good properties of the components and get rid of the bad ones [2]. Reinforcing metals with ceramics, invented by Schmidt in 1924 for an alumina particle reinforced aluminum composite [3], became popular in the second half of the twentieth century and for particle, and fiber reinforced composites were found applications in automotive [4], space [5], and aerospace [6], as well as in harsh environments, like chemical plants [7]. The development of metal matrix composites (MMC) promised an increase in the mechanical, thermal, and wear properties by reinforcing the metallic phase with a completely coherent ceramic phase [8]. The so-called interpenetrating metal-ceramic composites (IMCCs) have two topologically interconnected phases through the whole material. The interpenetrating combination of a light-weight metal and a very stiff ceramic promises high light-weight potential with very high

specific properties. This predicted increase in stiffness and compressive strength by Mattern et al. [8] was shown in various studies for the elastic range [9], the elastic–plastic range [10], as well as in in situ SEM [11] and CT studies [12] for the damage resistance.

Reasons why IMCCs are not broadly found in industrial applications yet are the lack of economic efficiency, resulting from the expensive preform production (cf. Scherm et al. [13] or Schreer et al. [14]) or a very time consuming in-situ manufacturing process [15]. A patented manufacturing process by Morgan Advanced Materials Haldenwanger GmbH reduces the preform manufacturing costs and makes the industrial application of IMCCs attractive [16]. Nevertheless, the success of the material depends also on the machinability and the cost of processing of the near net shape casted IMCC. The very brittle and hard alumina phase [17], combined with the ductile aluminum [18], challenges the machining process, as the difficult machinability is already known for aluminum-alumina MMCs in literature [19].

In principle, all machining processes like turning, milling, and drilling or unconventional processes like water jet machining (WJM), electrical discharge machining (EDM), electro-chemical machining (ECM), as well as hybrid processes like laser assisted machining (LAM) and ultrasonic assisted machining (UAM) can be used for the surface finishing of MMCs [20–23].

Advantages and disadvantages of those methods have been discussed in literature. Abrasive water jet cutting of Al-Al_2O_3 MMC tends to form a taper at the cutting edge [24]. For efficient ultrasonic assistant cutting process with the largest possible vibration amplitude, the mass- and geometry-dependent natural vibration frequencies for the system component (e.g., tool) must be determined. Due to the immense difference in the melting temperature of Al and Al_2O_3, laser cutting forms a large heat affected zone and dross at the exit of the cut surface [25].

The surface finish and surface integrity are important for surface-sensitive parts that are subjected to fatigue or creep. However, many machining methods often result in cracking, splintering and pulling out of the reinforcements. Grinding can be used to obtain a good surface finish and damage-free surfaces [19].

Grinding tools have numerous grain cutting edges of irregular size and shape; these tools are called undefined cutting edges. The tips and edges of grains act as cutting edges and are bond in a weak matrix material randomly all over the tool body. A large amount of micro-chipping effects of the engaging grains generates the total material removal in the grinding process. Thus, the total cutting load is distributed in a way that the load of a single grain is low. Using diamond grains, this process is suitable for cutting hard materials like ceramics, e.g., Al_2O_3 and SiC. Diamond grinding is also a well-established process to machine fiber reinforced ceramics with highly anisotropic and heterogeneous properties [26].

Hence, grinding is often limited to simple flat or cylindrical workpiece geometries. Grinding in a machining center uses a grinding head that replaces the milling tool to remove the workpiece material with a computer numerical control (CNC) milling machine [27].

1.1 Machining of MMC

Since research on the investigated interpenetrating metal ceramic composite, based on an open-cell Al_2O_3 preform, and a gas-pressure infiltrated AlSi10Mg alloy is extremely limited, some findings on the grinding of particulate reinforced MMCs are taken into account, as the combination of a brittle ceramic phase and a ductile metallic phase shows the basic challenge and first approaches for the machining and parameter finding discussed.

Most research studies focus on SiC-particulate reinforced aluminum composites (SiC_p/Al) with SiC volume fractions between 5 and 20% [27]. However, it must be noted that SiC reinforcement MMCs are even more difficult to machine than those reinforced with Al_2O_3. A common problem hereby are surface cracks in the matrix and the reinforcement, work hardened sub-surface, and the formation of voids and delamination which is due to pulled-out reinforced particles and aluminum matrix adhesion on the machined surface [27, 28].

Du et al. [29] analyzed the chip formation in machining of a SiC_p/Al composite. They called the process grinding, which is in our view equal to diamond grinding with the respective tool. It was found that the SiC particles inhibit the deformation of the aluminum matrix. The different contact positions between the SiC particles and the diamond grains cause the SiC particles to be fractured, pulled out, and/ or pushed into the surface of the chip.

Pai et al. [30] used a 35 vol.-% SiCp/Al composite in a comparable grinding process. It was found that the surface roughness improved with an increase in SiC volume percentage and decreased with the depth of cut. This was attributed to the increasing specimen hardness which decreases microploughing and positively influences the specific grinding energy.

When the grinding temperature exceeds 450 °C, a black color appears on the ground surface due to an oxidation reaction. According to Thiagarajan et al. [31], the residual compressive stress of such a burned surface layer is very high (cf. [27]). They proved that the grinding temperature increases with an increase in the cutting speed, feed rate, and depth of cut [31].

Hung et al. [28] investigated different grinding wheels in the grinding of a SiC_p/Al material with a SiC volume

content of 10 and 20%. The diamond wheels were more effective than the cubic Boron-Nitride (cBN) wheels since their grinding forces were lower and more stable. The diamond wheel showed a self-sharpening mechanism while the cBN wheel was pasted over with the soft aluminum matrix. This blocked the cutting grains and increased friction and thus grinding forces. A coarse-grit diamond wheel was deemed appropriate for rough grinding, and a fine-grit diamond wheel was deemed suitable for fine grinding to achieve the best surface integrity. Less effort was required to remove the thermally softened layer in rough grinding. The thermal softening effect was negligible in fine-grinding.

Kwak et al. [32] reported on different SiC and Mg volume contents and the influence of grain size and depth of cut on the surface roughness. However, the SiC and Mg volume contents and the grain size of the grinding wheel had little effect on the grinding force, while the machine table speed and the depth of cut were strongly affecting the grinding force [32]. Similar effects of the depth of cut and the feed rate on the grinding force were reported in Zhou et al. [33] and Chen et al. [27].

Zhao et al. [34] concluded that in grinding a SiC_p/Al material with a 63 vol.-% SiC content, a lower feeding speed, lower cutting depth, and a higher spindle speed should be chosen to obtain a better surface quality. To balance grinding efficiency and surface quality, a higher cutting depth at high cutting speed and reduced feed rate should be chosen.

1.2 Machining of IMCC

Besides the work done by Roy et al. [35] on the wire electrical discharge machining and Goswami et al. [36] on electrochemical grinding, little research has been done on conventional machining of Al_2O_3/Al interpenetrating phase composites (IPC) [36].

Liu et al. [37] investigated the use of an aluminum alloy with 15–40 vol.-% spinel and mullite foams for an application as a cut-resistant security material. Samples were cut using a diamond slitting wheel. Comparing spinel- and mullite-based IMCCs of similar volumetric reinforcement, the cutting resistance of the spinel-based IMCC was half of the cutting rate of the mullite-based IMCC. This difference in cutting resistance was attributed to the hardness of the spinel in comparison to the mullite. However, the 20% and 40% spinel IMCC had similar hardness values but showed a significant difference in the cutting rate. Therefore, it was believed that the hardness was not the only contributing factor to the cutting resistance. It was suggested that some of the aluminum phase is extruded and smeared across the surface, forming a strain hardened thin metallic layer in a manner similar to the drawing of metal. Consequently, it takes more effort to deform the aluminum phase in the cutting process. This effect would explain the observed brittle fracture of the aluminum.

Also, the ceramic phase was rarely observed at the surface since it was covered with a thin aluminum layer. It was assumed that this layer was created by the abovementioned smearing, although a secondary adhesion of metal debris could have also explained the effect. A crack was investigated that propagated along the ceramic grain boundaries and was bridged by the aluminum phase [37].

Although uncoated carbide tools are not very suited for processing materials containing silicon carbide [38], Karabulut et al. [39, 40] investigated an aluminum alloy with 40 vol.-% SiC foam in milling with such a tool. The tool showed excessive edge chipping which was attributed to sudden high-stress and relaxation phases when the hard SiC phase was cut and then suddenly released in the cutting area. A high temperature weakening of the bonding between the SiC and aluminum matrix was believed to result in the SiC phase breaking instead of cutting. The high temperature weakening of the bonding created small gaps, microcracks, and scratches on the surface which led to arithmetic mean roughness values (R_a) of between 1.9 and 3.2 µm. It was concluded that the SiC phase restricted the movement of the soft matrix and provided an "acceptable" surface quality. The feed rate was the most significant factor affecting the surface roughness, while the strongest influence on the cutting force was the cutting depth.

Prasanth et al. [41] investigated an aluminum alloy with 20 vol.-% SiC foam in end milling, using an uncoated carbide tool. They performed a grey relational analysis (GRA) following an experimental Taguchi investigation (cf. [42, 43]). The cutting speed and feed rate were the most important factors influencing the surface roughness and tool wear. The optimal parameters were found to be a cutting speed of 7000 rpm, a feed rate of 600 mm/min, and a depth of cut of 0.4 mm. The optimized parameters lead to a surface roughness of 1.08 µm and a tool wear of 18 µm after a tool travel of 0.1 m. However, it is not clear if the improved surface roughness reported was not due to smearing of the aluminum since no close examination of the machined surface was publicized.

As the state-of-the-art shows, the field of research on the machining of interpenetrating metal ceramic composites is still wide, and a lot of effort is to be taken, to understand the arising effects during machining, find suitable machining parameters, and optimize the processing for industrial application and successful transfer of this new material group form lab scale into industrial processes.

In this paper for the first time, the machinability of IMCC will be systematically investigated regarding machining parameters, the tool conditions, microstructural surface quality, and cutting forces. The machining experiments are carried out with small cylindrical tools to get an understanding

of processing of complex of complex geometries in near-netshape infiltrated metal-ceramic composites. CNC-machining process is the only manufacturing process for finishing of such near-netshape components like turbine blades, bearings, or other components, subjected to wear, thermal, or chemical environment.

Since it is strongly requested by one of the reviewers, we cite references here [44, 45] though they are absolutely irrelevant for the present work.

2 Material and methods

2.1 The interpenetrating aluminum-alumina composite material

The IMCC was manufactured via gas pressure infiltration with an AlSi10Mg alloy and a slurry-based alumina preform with 74% open porosity, provided by Morgan Advanced Materials Haldenwanger GmbH. A vacuum of $2 \bullet 10^{-2}$ mbar was used to evacuate the ceramic preform in a crucible with AlSi10Mg slabs, before the melt temperature of the aluminum alloy is exceeded at 700 °C. The metallic melt is infiltrated into the open porous structure of the alumina preform with an Argon gas pressure of 60 bar. The gas pressure infiltration process, as well as the microstructural characterization of the IMCC, was described elsewhere by the authors [9, 10].

A low residual porosity in the composite of 1 to 3% and a density of 2,95 g/cm^3 were measured [9]. An increase in specific stiffness of the IMCC compared with the aluminum alloy was determined and reaches up to 45%; the compression yield strength increased at room temperature from 198 to 365 MPa about 84%, as investigated by some of the authors [46, 47].

2.2 Sample preparation

For the grinding experiments, cuboid specimens with a dimension of 5 × 5x50 mm^3 were cut out of a material block with a diamond wire saw.

2.3 Hardness indentation measurement

For the indentation measurement, 5 × 5x5 mm^3 cubes were cut with a diamond wire saw of a material block and afterwards ground and polished. SiC grinding paper of P220 and P 500 were used, and a subsequential polishing program with 9, 3, and 1 µm diamond suspensions and a final polishing with a chemo-mechanical oxide polish OP-S suspension by Struers, Willich, Germany, were applied.

The hardness of the metallic and ceramic phase in the interpenetration composite was tested using a Duramin-40 micro-hardness tester from Struers, Willich, Germany. The test was carried out and evaluated after Vickers in accordance with the standard DIN EN ISO 6507–1. The holding time was 10 s, and the hardness scale "Vickers 0.3" with 0.3 kilopond (equivalent to 2.94 N) test force was used for evaluation. The hardness indentation was carried out specifically in a larger area of the metallic and ceramic phase so that the remaining hardness indentation was completely within the respective phase.

2.4 Grinding experiments

The grinding experiments were performed on the five-axis-machining center "DMG Ultrasonic 40 evo." During all machining experiments, external cooling with a water-based emulsion was applied. The specimens were fixed mechanically with a suitable device to allow side machining as displayed in the sketch of Fig. 1. Different process parameters

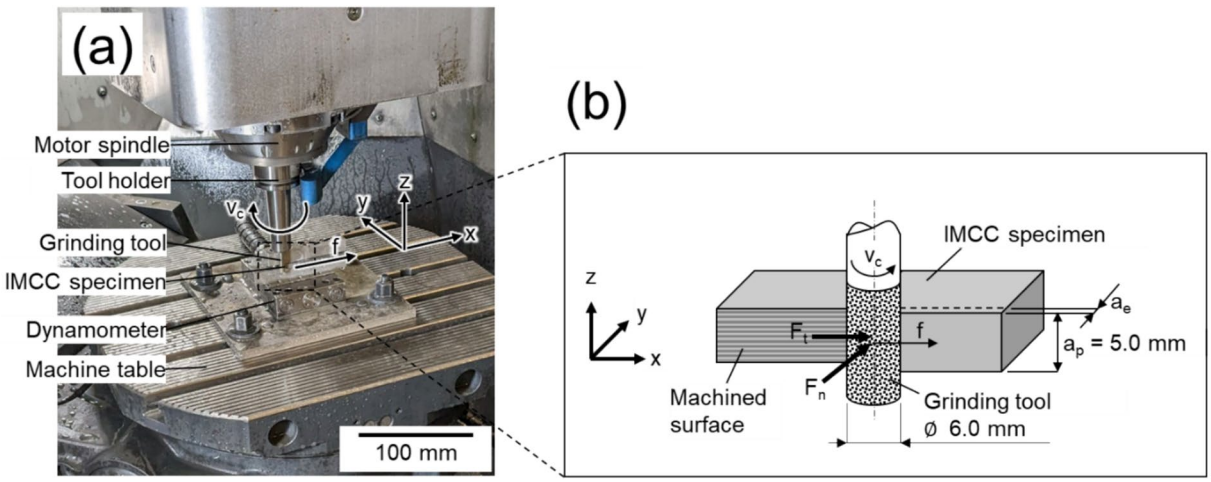

Fig. 1 Setup for grinding experiments on a machining center (**a**) image and (**b**) scheme of the machining conditions

were chosen (Table 1) and their influence on the tool quality; the cutting force and the surface quality of the parts were investigated. The cutting speed v_c is the rotation speed, and the feed rate f is the lateral machining movement per spindle revolution.

The tools were galvanic bonded diamond grinding tools of 6.0-mm diameter. The influence of the grain size was investigated for tools with D46, D126, and D251 grains. The corresponding average grain diameters are 45, 125, and 250 µm, respectively.

2.5 Cutting force measurement

The cutting forces of the grinding experiments were measured by a piezoelectric dynamometer (Kistler Type 911AA2) using a data acquisition frequency of 10 kHz. The force data was compensated for thermal drift. It is assumed that the tangential and normal forces, F_t and F_n, acting on the tool correspond to the measured force components. For each experiment, mean value and standard deviation from 10,000 single force values were determined.

2.6 Surface topography characterization methods

The surfaces roughness was analyzed by the focus variation method (Alicona Infinite Focus). According to DIN EN ISO 25178 the 3D-roughness parameter S_a (arithmetic mean roughness) was determined from a measurement area of 3×3 mm^2 and by applying a robust Gaussian filter (cut-off 0.6 mm). The number of roughness measurements of each test series was three. For microstructure analysis of the machined surfaces, scanning electron microscope (SEM) Prisma E SEM by ThermoScientific, Waltham, USA was used. The surfaces of the grinding tools were investigated by light microscope (Keyence VHX-5000).

3 Results

In the following, the results of this study are given for the material characterization, as well as for the mechanical machining processes. Hardness indentation measurements, the influence of the tool choice, the grinding kinematic, and the cutting depth are addressed.

3.1 Hardness indentation measurement

The challenge in the hardness testing of a multi-phase material is that the two material phases exhibit a very clear difference in hardness, and therefore hardness measurements over a larger range always depends on the phase proportion ratio. The indentations were made in the homogeneous ceramic or metallic phase. Images of the hardness indentation can be seen in Fig. 2. The hardness of the metallic phase was approx. 70 HV0.3 and the hardness of the ceramic phase 1900 HV0.3. The indentations had an unequal aspect ratio of 0.98 for the metallic hardness indentation and 0.88 for the ceramic hardness indentation.

3.2 Influence of the tool grain size

One key performance factor of grinding tools is the grain size. Increasing grain size allows higher chip thickness and therefore a grinding process with higher material removal rate. Surface roughness is expected to increase with increasing grain size in homogeneous materials, as the distance between the active grain edges is larger and grains stand further out of the bond.

On the IMCC material grinding, experiments were carried out with galvanic bonded tools with three different diamond grain sizes. Figure 3 summarizes the effect of the grain size on the cutting forces and surface roughness. Tangential and normal forces as well as the arithmetic mean roughness for the grain sizes 45, 125, and 250 µm with the corresponding feed rates 23, 63, and 126 µm/rev are shown. Increasing grain size and feed rate by factor 5.5 lead to increases of the tangential force of 108% (5.1 to 10.6 N) and the normal force of 70% (13.7 to 23.3 N). The roughness value S_a shows a quite similar increase of 78% (4.46 to 7.94 µm). This can be explained by the surface topographies of the machined IMCC specimens in Fig. 4, which illustrates the grooves along the grinding direction left by the rotating grains. With increasing grain size, the distance increases and the depth and width of the grooves increases obviously.

Table 1 Fixed and variable machining process parameters

Fixed parameters		Variable parameters	
Parameter	Value	Parameter	Levels
Axial infeed	5.0 mm	Tool: Diamond grain size/µm	45, 125, 250
Coolant flow rate	40 l/min	Grinding directions	Up- and down-grinding
Coolant pressure	4 bar	Feed rate f/µm/revolution	31.5, 63, 47, 79, 126
Coolant type	Water-based emulsion	Cutting speed v_c/m/min	113, 160, 255, 302, 349, 396
		Cutting depth a_e/mm	0.05, 0.10, 0.20, 0.35, 0.50

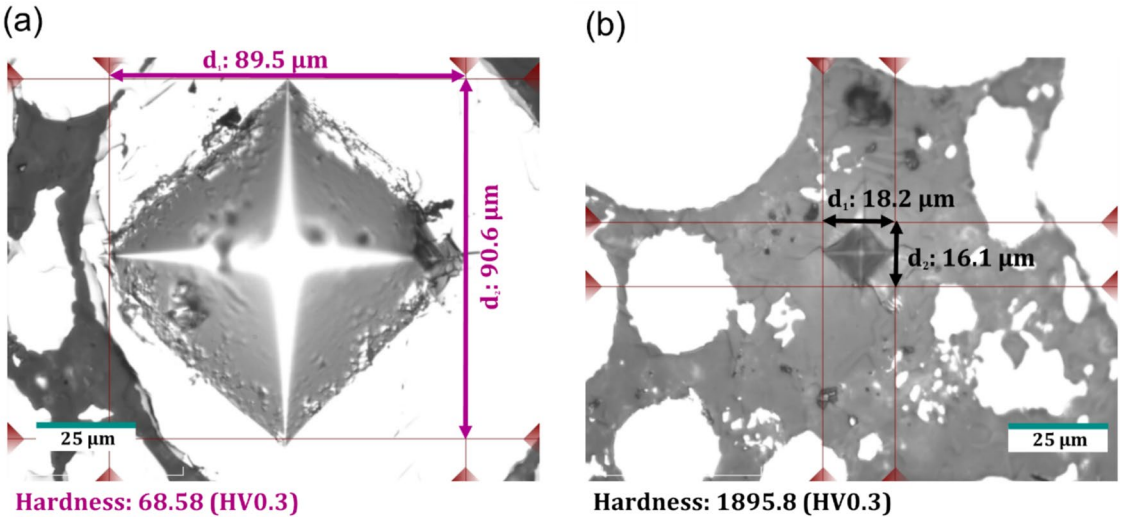

Fig. 2 Remaining indentation after the hardness test with a HV0.3 test specimen (**a**) in the bright, metallic surface and (**b**) in the gray, ceramic surface (right). The corresponding information is given below the pictures

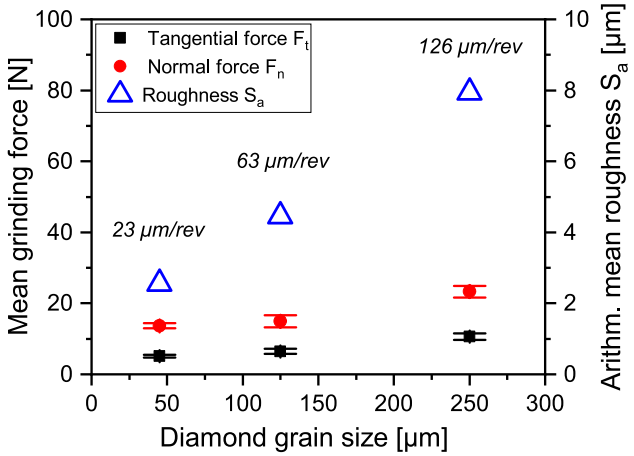

Fig. 3 Mean tangential and normal grinding force and arithmetic mean roughness dependent on the diamond grain size of the grinding tool of 45, 125, and 250 µm processed by the corresponding feed rates of 23, 63, and 126 µm/rev

The grain size also influences the tool surface and its performance. The SEM images of Fig. 5 show diamond tool surfaces of fine grain (45 µm) and coarse grain (125 µm). The diamond grains are bonded galvanically by a metallic nickel-based matrix. After a grinding distance of just 50 mm, the deposition of grinding chips on the grinding tool surface is obvious. While at a grain size of 45 µm, areas of several square millimeters are already covered by chips, at a grain size of 125 µm, only scattered grain spaces are affected.

3.3 Influence of the grinding direction

The cutting direction describes the direction in which the chips are removed, i.e., how the directions of the cutting and feed movements relate to each other. Like in Fig. 6(a) is presented schematically, in down-grinding, the grain cut from the upper edge of the workpiece with maximum

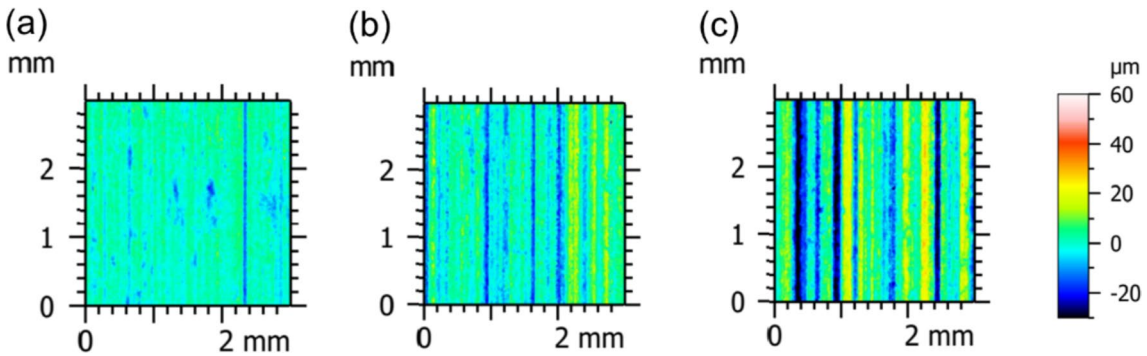

Fig. 4 Surface topographies of machined specimens at 207 m/min for diamond grain sizes of (**a**) 45 µm, (**b**) 125 µm, and (**c**) 250 µm

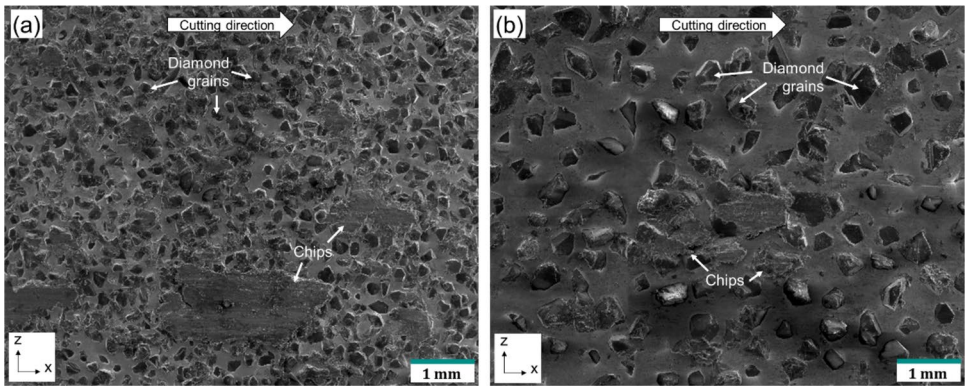

Fig. 5 SEM images of the grinding tool surfaces after a cutting distance of 50 mm for the diamond grain size of (**a**) 45 µm and (**b**) 125 µm

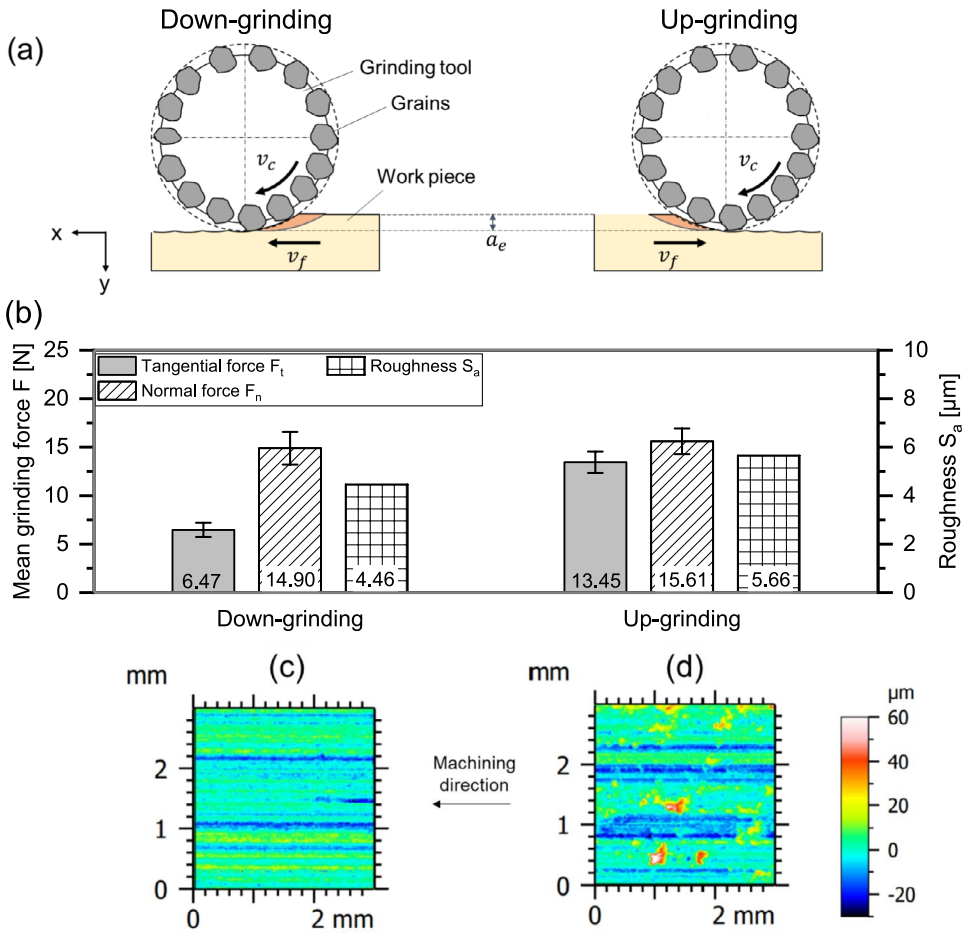

Fig. 6 (**a**) Schematic down- and up-grinding; **b** Influence of the grinding direction on mean tangential and normal grinding force and artihmetic mean roughness; surface topographies of machined specimens at 207 m/min and 63 µm/rev: **c** Down-grinding and (**d**) Up-grinding

chip thickness to the bottom with a chip thickness of zero. The opposite is the up-grinding. Figure 6b compares the grinding forces and surface roughness S_a of down- and up-grinding process. Down-grinding shows significant lower tangential forces and almost equal normal force. Down-grinding has 21% lower S_a-value than up-grinding. Figure 6c and d give the information about the topography of the processed IMCC surfaces. Additional to the typical grinding grooves, which is obvious for both machining directions, up-grinding shows also topographic peaks of up to 60 µm higher than the surface plateau. These are metal depositions, which is shown by the SEM image of the machined surface after up-grinding in Fig. 7b. Furthermore, it shows chipping of the ceramic phase and plasticizing of the metal phase, which is the same for down-grinding in Fig. 7a.

As the tangential force of up-grinding is much higher than of down-grinding, and the chip formation and roughness

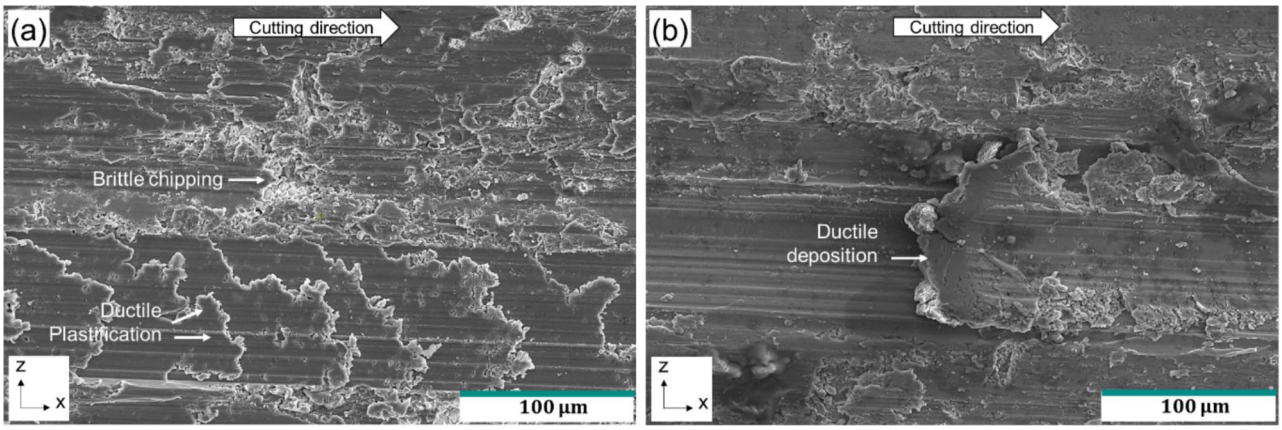

Fig. 7 SEM images of the machined IMCC surfaces for (**a**) down- and (**b**) up-grinding

peaks are much more significant, we would recommend to use down-grinding.

3.4 Influence of grinding kinematic and cutting depth

The grinding kinematics is a superposition of rotary and feed movements which can be varied by cutting speed v_c and feed rate f respectively. The cutting depth a_e is another important grinding parameter, which effects the chip thickness. All tests were done by down-grinding and with tools with a diamond grain size of 125 µm. Figure 8 presents the normal and tangential forces during grinding of the IMCC material for cutting speed v_c, feed rate f and cutting depth a_e.

Cutting speeds between 113 and 396 m/min show an almost constant behavior of both tangential force F_t (approx. 7 N) and normal force F_n (approx. 17 N). On the other hand, increase forces linear with increasing feed rates, which has been expected and observed also in other grinding and milling operations [38]. Between 31.5 and 126 µm/rev F_t as well as F_n are increased by factor 4. An increase of the cutting depth a_e from 0.05 to 0.5 has even higher impact on the forces, resulting in F_t increasing degressively from 4.2 N to 15.9 N and F_n increasing as well from 10.7 N to 81.9 N.

There seems to be no influence on the machined surfaces by means of arithmetic mean roughness S_a due to the investigated variations of cutting speed, feed rate, and cutting depth (Fig. 9). However, comparing the surface topographies of the machined specimens, like in Fig. 10, there are differences along grinding direction. Compared with grinding with cutting speed of 113 m/min, feed rate of 63 µm/rev, and cutting depth of 0.10 mm (Fig. 10a), increasing the cutting speed to 396 m/min (Fig. 10b), double the feed rate to 126 µm (Fig. 10c), and increasing the cutting depth to 0.50 mm (Fig. 10d) lead to more frequent interruptions of the grinding grooves. All height profiles are in the same range. Figure 11 shows the microscopic images of the corresponding tool surfaces. Only the grinding tool which was used at moderate grinding conditions (Fig. 11a) has no changes. Increasing cutting speed, feed rate, and cutting depth (Fig. 11b–d) lead

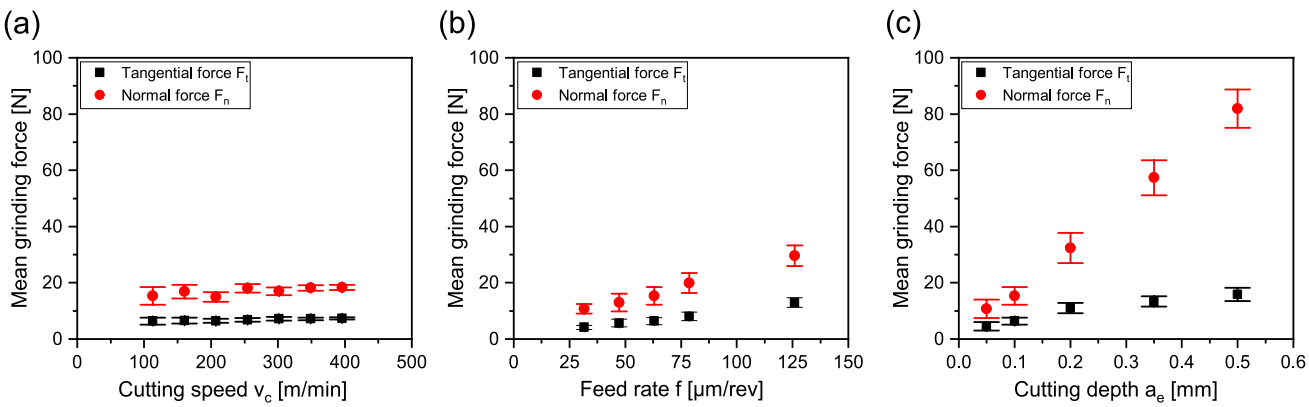

Fig. 8 Normal and tangential grinding forces dependent on (**a**) cutting speed, **b** feed rate, and (**c**) cutting depth

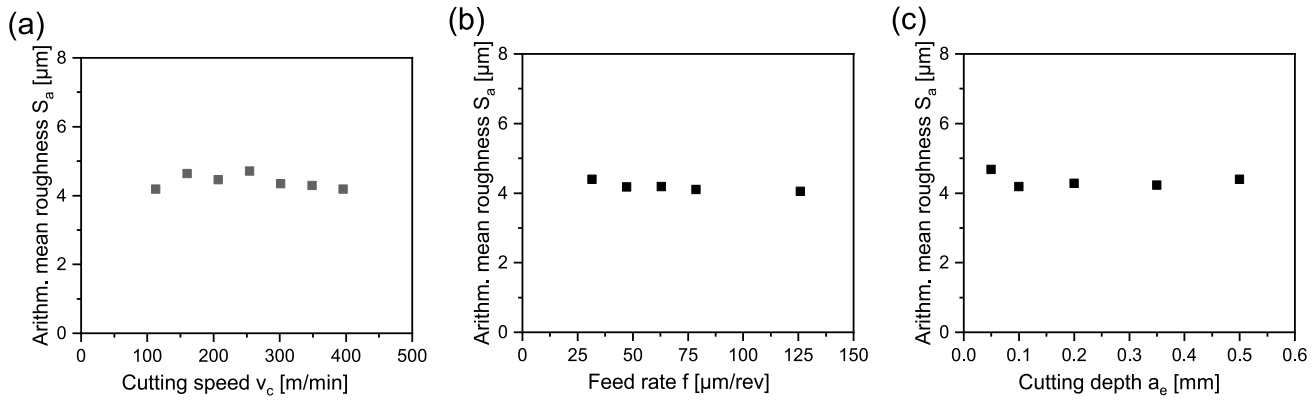

Fig. 9 Mean roughness dependent on (**a**) cutting speed, **b** feed rate, and (**c**) cutting depth

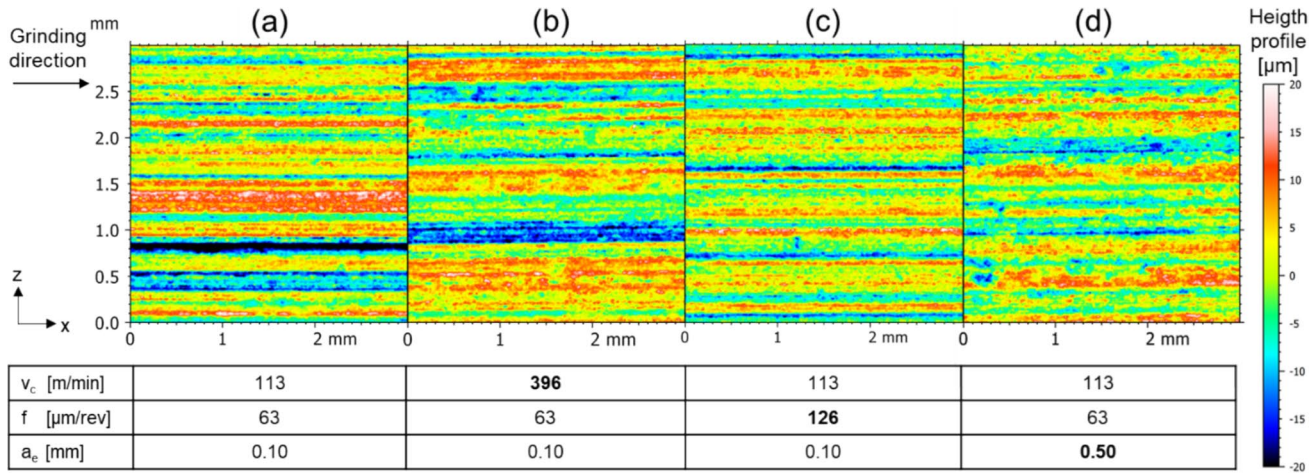

	(a)	(b)	(c)	(d)
v_c [m/min]	113	**396**	113	113
f [µm/rev]	63	63	**126**	63
a_e [mm]	0.10	0.10	0.10	**0.50**

Fig. 10 Surface topographies of machined specimens with different grinding parameters (cf. table below the images): (**a**) v_c = 113 m/min, f = 63 mm/rev, and a_e = 0.10 mm; (**b**) v_c = 396 m/min, f = 63 mm/rev, and a_e = 0.10 mm; (**c**) v_c = 113 m/min, f = 126 mm/rev, and a_e = 0.10 mm; (**d**) v_c = 113 m/min, f = 63 mm/rev, and a_e = 0.50 mm

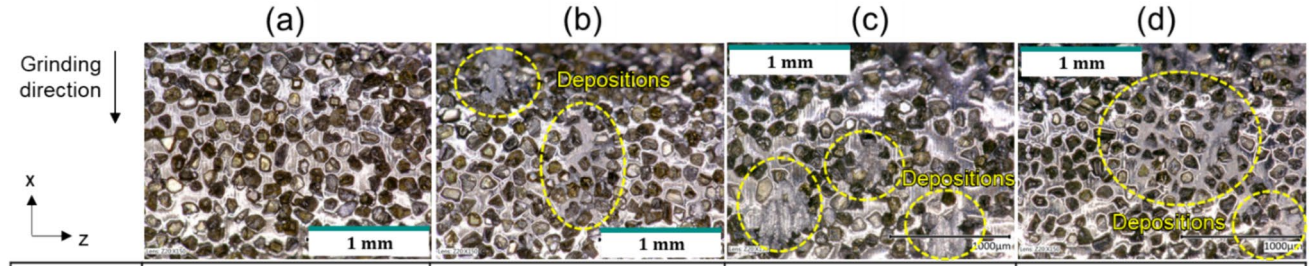

	(a)	(b)	(c)	(d)
v_c [m/min]	113	**396**	113	113
f [µm/rev]	63	63	**126**	63
a_e [mm]	0.10	0.10	0.10	**0.50**

Fig. 11 Grinding tool surfaces after a grinding distance of 50 mm with different grinding parameters (cf. table below the images): (**a**) v_c = 113 m/min, f = 63 mm/rev, and a_e = 0.10 mm; (**b**) v_c = 396 m/min, f = 63 mm/rev, and a_e = 0.10 mm; (**c**) v_c = 113 m/min, f = 126 mm/rev, and a_e = 0.10 mm; (**d**) v_c = 113 m/min, f = 63 mm/rev, and a_e = 0.50 mm

to metal depositions on the tool surface already after a grinding distance of 50 mm.

The efficiency of these grinding processes is first of all directly related to the material removal rate and secondly to the cutting power. The received surface roughness can give an information about the machining quality.

The cutting power P_c is the product of the tangential force F_t and the cutting speed v_c. A correlation between increasing P_c and decreasing S_a can be supposed, for the plot of cutting power over the surface roughness (see Fig. 12a), with a measured surface roughness between 4 and 5 µm. This effect is more present for cutting speed or feed rate than for cutting depth. Figure 12b and c compare the surface topographies of the IMCC after grinding with feed rates of 31.5 and 126 µm/rev, as the roughness value S_a decreases from 4.39 to 4.05 µm, while the calculated cutting power P_w increases from 7.84 to 24.52 W. For a feed rate of 31.5 µm/rev, the topography has grooves along the grinding path from − 20 to + 20 µm. Increasing the feed rate to 126 µm, the profile valleys are only up to 10 µm, and the profile elevations in y-direction are wider.

Figure 13 shows the effects of surface formation by means of SEM images of the machined IMCC surfaces. The surface at a feed rate of 63 µm/rev shows breakouts and elevations as

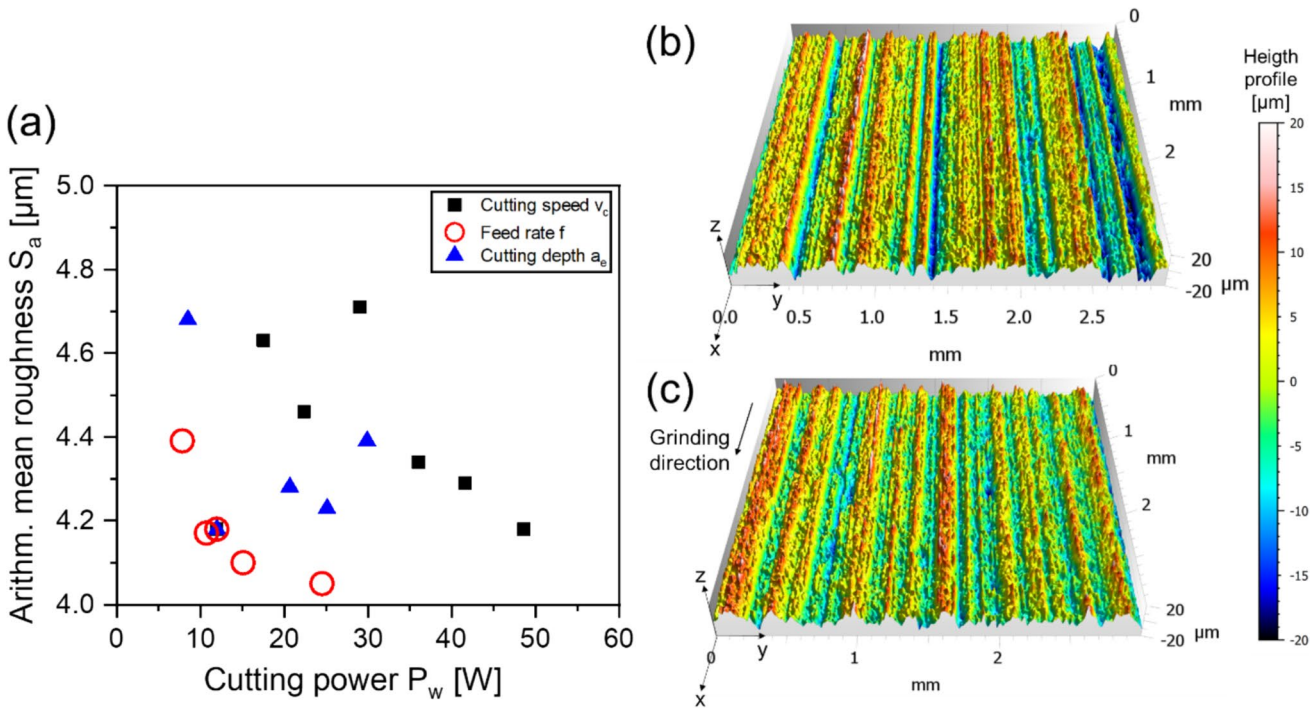

Fig. 12 (**a**) Cutting power dependent on the arithmetic mean roughness and the surface topographies at feed rates of (**b**) 31.5 and (**c**) 126 mm/rev

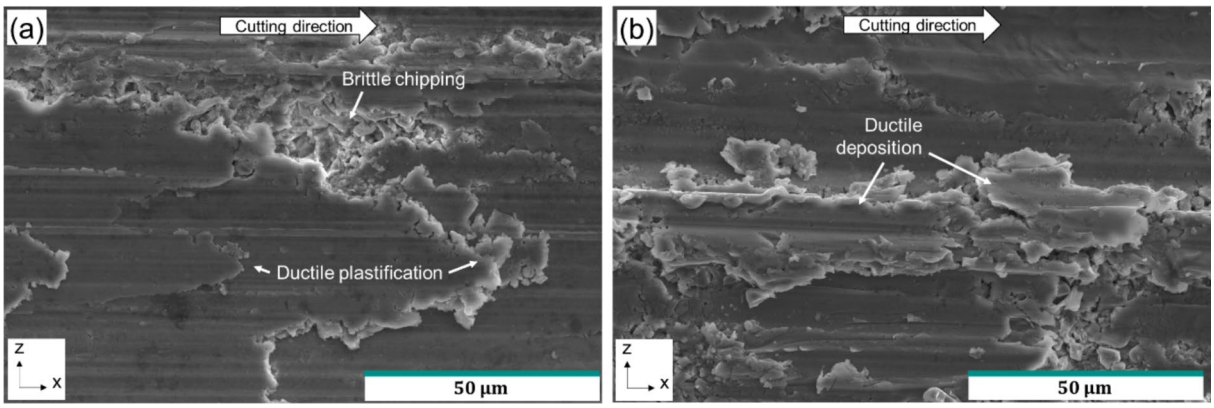

Fig. 13 SEM-images of the machined IMCC surfaces for feed rates of (**a**) 63 µm/rev and (**b**) 126 µm/rev

well. Increasing the feed rate to 126 µm/rev reduces breakout and leads to more prominent elevations.

Figure 14 shows the influence of the material removal rate Q_w on the cutting power P_c. While increasing Q_w by increasing the cutting speed and the feed rate leads to a linear increase of cutting power, an increase of the cutting depth shows a degressive growth of cutting power P_c.

4 Discussion

4.1 Influence of grinding parameters on the cutting forces

During grinding, the mechanical energy is almost completely converted into heat. A large part of this generated heat flows into the workpiece [48].

Therefore, the cutting forces are important indicators of the heat input during the process. The grinding process was investigated by evaluating the tangential and the normal cutting forces (F_t and F_n) dependent on diamond grain size of the grinding tool, cutting direction (up-grinding and down-grinding), cutting speed v_c, feed rate f, and cutting depth a_e. The corresponding results are plotted in Fig. 3, Fig. 6b, and Fig. 8a–c. For the grinding of IMCC, normal force is considerably higher than tangential force. This was expected, as monolithic Al_2O_3 [49] or metal aluminum [50] as well as different particle reinforced metal matrix composites like SiC/Al [51] or TiC/Ti [52, 53] behave in the same way. The material removal as well as the measured forces during grinding is made up of all single removals of the grain cutting edges. These grain cutting edges in turn have irregular shape, arrangement and number, resulting in irregular chip size and thickness (the so-called tools with geometric undefined cutting edges). The nature of cutting with grains results in negative rake angles, which leads to higher normal, than tangential forces.

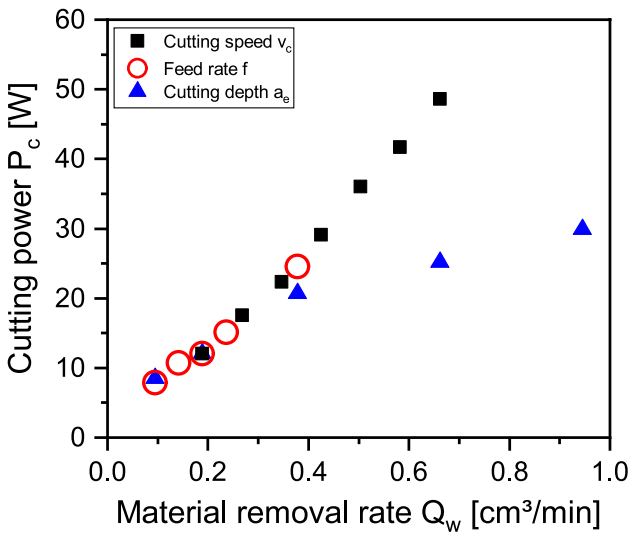

Fig. 14 Cutting power over the material removal rate

While the cutting speed v_c has no influence on the cutting forces, increasing feed rate f and radial infeed a_e leads to an almost linear increase of both F_t and F_n. These results are consistent with recent work on grinding forces, since changes in F_t and F_n can be related to changes of the undeformed chip thickness for variation of feed rate and radial infeed [54].

$$\bar{h}_{max} = 0.694 \cdot \left(\frac{2}{C_1 \cdot \tan\alpha}\right)^{\frac{1}{3}} \cdot \left(\frac{v_f}{v_c}\right)^{\frac{1}{3}} \cdot \left(\frac{a_e}{d}\right)^{\frac{1}{6}} \quad (1)$$

Due to material removal by multiple engagements of grains as well as the irregular shape and position in the grain cutters, for grinding, it is only possible to determine a mean undeformed chip thickness $\bar{h}_{max}$ [55].

The mean maximum chip thickness $\bar{h}_{max}$ can be described statistically and depend on the tool-related variables (C1, α), the movement variables (v_c, v_f) and the geometric conditions (a_e, d).

During longitudinal grinding, the feed movement is parallel to the work piece surface at the feed speed v_f. The feed rate f is moved by each spindle revolution n [56]. For the spindle turning n, one can also substitute the cutting speed v_c divided through π times the tool diameter d.

$$v_f = n \cdot f = \frac{v_c}{\pi \cdot d} \cdot f \quad (2)$$

Therefore, an increase of the feed rate f is direct related to the feed speed v_f and leads to an increased mean undeformed chip thickness as well as higher process forces, like in Fig. 8b. The same applies to increasing the cutting depth in Fig. 8c. For a_e, the increase is stronger because the investigated range from 0.05 to 0.50 mm is with factor 10 higher, than for f (factor 4).

The cutting speed is generated by the tool rotation and determines the actual speed of the chip removal process. In contrast to previous investigations on grinding [49, 50], not the feed speed and the material removal rate but the feed rate is kept constant in order to avoid the influence of the chip geometry. If the cutting speed increases, this is obtained by increasing the feed rate accordingly, which also increases the material removal rate. Figure 8a shows almost constant tangential and normal cutting forces, which also means that there is no change of the material removal behavior between 113 and 396 m/min. This can be classified as process typical behavior, since the grinding of carbon fiber-reinforced silicon carbide shows a similar behavior of the force curves [38].

The cutting direction, conversely, has a significant influence on the tangential grinding force F_t of the IMCC. While the normal force F_n is in the same range, F_t is twice as large during up-grinding (Fig. 6b). Like Fig. 6a shows, during up-grinding, very small chip thicknesses are present directly after the grain cutting edges enter the material. Elastic and plastic deformations initially occur, which lead to a compaction of the material structure. The material chipping starts once a critical chip thickness has been exceeded. The energy input for the elastic and plastic deformations only contributes indirectly to material separation. This can be minimized with increasing chip thickness, which is more favorable in terms of energy. This must be the case with down-grinding, as the maximum chip thickness of the abrasive grain is already present when it hits the upper edge of the material. This is consistent for example with the results of previous investigations on the grinding of SiSiC and ZrO_2 [49, 57]. Comparative results on machining of Al/Al_2O_3 interpenetrating phase composites are not found in literature, as mentioned in the introduction.

The grinding performance can be expressed, e.g., by the material removal rate and depends on the process parameters but also on the tool design. Increasing the diamond grain size of the grinding tool and increasing the feed rate by the same factor lead to a progressive increase of the cutting forces (Fig. 3). However, this is particularly due to the increase in the feed rate (compare with Fig. 8b). Compared with the 45 µm diamond grains, a diamond size of 125 µm shows just small increases of F_t (22%) and F_n (8%), but the 250-µm grains have much larger increases of F_t (108%) and F_n (70%). This means that the process forces do not change a lot between tools with grain sizes of 45 and 125 µm, although the feed rate and therefore the material removal rate is increased by factor 2.7.

4.2 Influence of grinding parameters on the IMCC surface topography and microstructure

The machined IMCC surfaces are discussed by roughness S_a, surface topographies and SEM-images of the microstructure.

The behavior of the arithmetic mean roughness S_a over the diamond grain size seems to be quite linear. The change of the roughness value is particularly due to the variation in grain size, because the feed rate has hardly any influence on the roughness (compare with Fig. 9b). There is an increase from 4.46 µm (grain size 45 µm) to 7.94 µm (grain size 250 µm). The corresponding surface topographies in Fig. 4 show the reason for this effect. With larger grain size, the tools generate deeper and wider grooves along grinding direction into the work piece surface. These tool-induced markings result from the ductile cutting behavior of the aluminum.

Hence, the roughness of machined Al_2O_3 particle reinforced aluminum, which was ground by grinding wheel with a grain size of 60 µm, is with R_a of 0.2–0.7 µm an order of magnitude lower [19]. These particles are in micrometer size and well distributed in the metal matrix, while in contrast, the IMCC in this study has larger areas of ceramic Al_2O_3 due to the interpenetrating ceramic foam structure.

Any further investigations were performed by a tool with 125 µm grain size. This includes the influence of the grinding direction. Like the grinding force, also the roughness value S_a is lower for down-grinding than for up-grinding (Fig. 6b). Compared with down-grinding, the surface topography of up-grinded IMCC in Fig. 6d shows additional typical grinding grooves between a profile height range from − 20 up to + 20 µm randomly distributed elevations, which have a peak height of up to 60 µm. By the microstructure in Fig. 7b, this is identified as aluminum depositions. In up-grinding, very small chip thicknesses are present directly after the entry of the grain cutting edges. Elastic deformations (high normal forces) and strong friction effects (high tangential force) are present at first. Only after a critical chip thickness is exceeded, shearing of chips occurs for the metallic aluminum due to plastic deformation, while cracking leads to brittle removal of the Al_2O_3.

The energy input for elastic deformation only contributes indirectly to material removal. If these can be reduced with larger chip thicknesses, this leads to energetically more efficient material removal conditions. This must be the case with down-grinding, as the mean maximum chip thickness is already reached when the abrasive grain hits the material. In addition, reduced friction results in lower energy conversion, grinding forces and therefore in lower heat input.

The microstructures of the ground IMCC in Fig. 7 both show a continuous structure of a flake-like pattern in cutting direction due to plastically deforming of the metal aluminum. The higher heat input during up-grinding leads to chip accumulations on the tool surface and finally to a cold-welding of the chips on the composite material surface, resulting in depositions and higher surface roughness. Therefore, investigations of the grinding kinematic and cutting depth were done by down-grinding.

Cutting speed v_c, feed rate f and cutting depth a_e, shown in Fig. 9, have a constant surface roughness S_a of approx. 4.5 µm. Nevertheless, the feed rate f and cutting depth a_e show significant influence on the grinding force in Fig. 8 due to the change of the "undeformed chip size," which leads also to a change of the heat conditions.

In contrast to the roughness values, the surface topographies in Fig. 10 show differences for changes in cutting speed from 113 to 396 m/min, in feed rate from 63 to 126 µm/rev and in cutting depth from 0.1 to 0.5 mm. Compared with a setup with moderate grinding conditions in Fig. 10a present the IMCC surface textures after machining with increased parameters in Fig. 10b–d local interruptions of the distinct parallel oriented grinding grooves in cutting

direction as well as crest flattening. This results from localized flow of material, which is obvious in Fig. 13b, when analyzing the microstructural surface texture ground at f = 126 µm/rev. In Fig. 13a, more metal aluminum is plasticized, looking like ductile depositions, because of increased cutting temperature compared with grinding with lower feed rate. In turn, this leads also to a reclosing of defects from brittle ceramic chipping. Here, the significant difference in hardness between the two interpenetrating phases becomes apparent, as measured in the hardness indentation measurement (cf. Fig. 2). The high hardness of the alumina phase with approx. 1900 HV0.3 does not show a damage tolerant behavior and breaks brittle, without a plastic elongation at break. The soft aluminum with approx. 70 HV0.3, only, is removed in a ductile way and recloses surface defects (cf. Figs. 7, 10, and 13). In mechanical testing, the specific phenomena of each phase and their interaction in the IMCC can be observed [9, 46]. Zan et al. [58] and Mypati et al. [21] describe the material removal mechanisms of MMC as a combination of localized plastic deformation and brittle fracture. This also applies to the IMCC, although the ductile material removal mechanisms are more prevalent compared to the brittle ones. This is because the material volume proportions of AlSi10Mg alloy and Al_2O_3-ceramic are approx. 3:1.

For cutting speed, feed rate and cutting depth variations the S_a-values in Fig. 12a seem to have an indirect correlation to the cutting power P_c, indicating the induced thermal process energy. The influence on the surface texture is demonstrated by 3D-surface topographies in Fig. 12b and c. Increasing the feed rate from 31.5 to 126 µm/rev increases also the cutting power and leads to a topography with decreasing profile height, confirming the ductile plasticizing as well as the reclosing effects of brittle induced defects (fractured and splintered ceramic).

4.3 Influence of grinding parameters on the tool and the machining performance

Higher thermal process energy at increasing cutting speed, feed rate, or cutting depth also leads to faster tool wear. Just after grinding distance of 50-mm local metal depositions on the tool surface are obvious (Fig. 11b–d). These depositions are confirmed by Marousi et al. [23], who observed already after a few seconds of cutting MMC a significant amount of adhering material forming a built-up edge on the tool.

If the chip spaces between the grains of a grinding tool are covered with chips, the grains in these areas will no longer take part in the cutting process anymore. The remaining cutting grains have to compensate for this and are subject to additional stress during grinding. With ongoing depositing of chips and increasing sealing of the grinding tool surface, the material is increasingly unable to be removed resulting in loss of process stability. In contrast, the tool surface of grinding with moderate cutting parameters in Fig. 11a shows no change.

The aluminum depositions on the tool surface are even more severe if the grain size is reduced, because smaller grains have smaller distance, stand out less from the bonding, and have smaller chip spaces. Figure 5a shows for the 45 µm grain size already after 50-mm grinding distance large areas of the tool surface covered with such aluminum depositions, while the 125 µm grain size is still almost free of it.

If tools with smaller grain sizes still have to be used because lower roughness is required, these must be applied at decreased process speeds and cutting depth in order to achieve acceptable tool life. Although this reduces the material removal rate and hence the efficiency. If the other way round, the material removal rate is increased, like in Fig. 14, the most energetically way with the lowest heat generation is to increase the cutting depth instead of cutting speed and feed rate. Although, the tool wear increases at high cutting depth. This confirms the complexity of the removal behavior of the IMCC material system. Although further investigations are required for a quantitative description, this work has already qualitatively identified various effects.

5 Summary and conclusion

In this study, machining experiments of an interpenetrating metal-ceramic composite were done with a machining center to investigate the machinability, which is required for the development of an industrial machining process for IMCC components. Grinding experiments were performed with diamond grinding tools (diameter 6.0 mm) with respect to different grain sizes and cutting direction. The influence of the process kinematic was investigated at cutting speeds between 113 and 396 m/min and feed rates between 31.5 and 126 µm/rev. The cutting depth was varied between 0.05 and 0.5 mm.

The principle cutting mechanisms of IMCC is a combination of brittle fracturing of the Al_2O_3-ceramic phase and plastically deforming of the metal aluminum. These effects increase if more heat is induced during processing at increased cutting forces and leads to a reclosing of defects from brittle ceramic chipping. This occurs when increasing material removal rate due to cutting speed, feed rate, or cutting depth resulting in a slightly decrease of the surface roughness S_a, like from 4.39 to 4.05 µm for increasing feed rate between 31.5 and 126 µm/rev.

Higher heat input also leads to more metal aluminum depositions on the grinding tool surface. These depositions are even more sever for smaller grain size like 45 µm, because compared with 125 µm grain size, the tool is covered much faster and increasingly unable to show stable

grinding performance. If significant lower surface roughness is required, this is nevertheless only possible through smaller grain size.

The largest aluminum depositions on IMCC surface is generated by up-grinding process. This is due to the higher process forces and therefore heat input compared to down-grinding, which is the preferred grinding direction.

Acknowledgements We want to thank Morgan Advanced Materials Haldenwanger GmbH for the friendly supply of complimentary preform material, Christian Beck for his participation as bachelor student, and Joshua Macken for the support of the experiments in this project.

Author contribution All authors contributed to the study conception and design. Material preparation, data collection, and analysis were performed by Achim Rösiger and Joél Schukraft. The first draft of the manuscript was written by Achim Rösiger and Joél Schukraft. All authors commented on previous versions of the manuscript and read and approved the final manuscript.

Funding Open Access funding enabled and organized by Projekt DEAL. This collaborative research between the University of Applied Sciences Augsburg and the Augsburg University is part of an internal research project of the THA_comp research group from the Technical University of Applied Sciences Augsburg and was gratefully supported financially by the German Research Foundation (DFG) within the project WE 4273/17–1.

Declarations

Competing interests The authors declare no competing interests.

References

1. Immanuel R, Panigrahi S, Malas J (2023) Materials development for sustainable manufacturing. In: Sustainable Manufacturing Processes, Elsevier
2. Ashby MF (2005) Materials selection in mechanical design, 3rd edn. Elsevier Science & Technology, Oxford
3. Schmidt E (1924) Herstellung Aluminiumartiger Werkstücke und Baustoffe und Behandlung von Leichtmetallen DE425451; DE425452
4. Lenke I, Richter G,Rogowski D (2001) Ceramic engineering with preforms for locally reinforced light metal components, In: ceramic materials and components for engines, Heinrich JG, Aldinger F, eds., Wiley-VCH Verlag, Weinheim GmbH, Germany.
5. Rawal S (2001) Metal-matrix composites for space applications. JOM 53:14–17. https://doi.org/10.1007/s11837-001-0139-z
6. Miracle D (2005) Metal matrix composites - from science to technological significance. Compos Sci Technol 65:2526–2540. https://doi.org/10.1016/j.compscitech.2005.05.027
7. Asthana R, Kumar A, Dahotre NB (2006) Materials processing and manufacturing science. Elsevier, Amsterdam
8. Mattern A, Huchler B, Staudenecker D, Oberacker R, Nagel A, Hoffmann M (2004) Preparation of interpenetrating ceramic-metal composites. J Eur Ceram Soc 24:3399–3408. https://doi.org/10.1016/j.jeurceramsoc.2003.10.030
9. Horny D, Schukraft J, Weidenmann K, Schulz K (2020) Numerical and experimental characterization of elastic properties of a novel, highly homogeneous interpenetrating metal ceramic composite. Adv. Eng. Mater 22. https://doi.org/10.1002/adem.201901556
10. Schukraft J, Horny D, Schulz K, Weidenmann K (2022) 3D modeling and experimental investigation on the damage behavior of an interpenetrating metal ceramic composite (IMCC) under compression. Mater Sci Eng: A 844. https://doi.org/10.1016/j.msea.2022.143147
11. Morbitzer P, Schukraft J, Lohr C, Weidenmann K (2023) In-situ SEM investigation on the damage behavior of an interpenetrating metal ceramic composite. Compos Structures 321. https://doi.org/10.1016/j.compstruct.2023.117278
12. Schukraft J, Lohr C, Weidenmann K (2021) 2D and 3D in-situ mechanical testing of an interpenetrating metal ceramic composite consisting of a slurry-based ceramic foam and AlSi10Mg. Composite Structures 263. https://doi.org/10.1016/j.compstruct.2021.113742
13. Scherm F, Völkl R, Neubrand A, Bosbach F, Glatzel U (2010) Mechanical characterisation of interpenetrating network metal-ceramic composites. Mater Sci Eng, A 527:1260–1265. https://doi.org/10.1016/j.msea.2009.09.063
14. Schreer K, Roth I, Schneider S, Ehnis H (2014) Analysis of aluminum and steel pistons–comparison of friction, piston temperature, and combustion. Journal of Engineering for Gas Turbines and Power 136:136. https://doi.org/10.1115/1.4027275
15. Breslin M, Ringnalda J, Xu L, Fuller M, Seeger J, Daehn G, Otani T, Fraser H (1995) Processing, microstructure, and properties of co-continuous alumina-aluminum composites. Mater Sci Eng, A 195:113–119. https://doi.org/10.1016/0921-5093(94)06510-1
16. Lavrentyeva O (2016) Verfahren zur Herstellung von aufgeschäumten keramischen Werkstoffen sowie dadurch herstellbarer keramischer Schaum. DE102015202277A. https://www.freepatentsonline.com/DE102015202277.html
17. Software (2020) Material database: Alumina 99,95 \%. Granta EduPack, Ansys Inc, Canonsburg, PA, USA. https://www.ansys.com/
18. Software (2020) Material database: Aluminium A360.0, die cast F. Granta EduPack, Ansys Inc, Canonsburg, PA, USA. https://www.ansys.com/
19. Zhong Z, Hung N (2002) Grinding of alumina/aluminum composites. J Mater Process Technol 123:13–17. https://doi.org/10.1016/S0924-0136(02)00075-4
20. Davim JP (ed) (2014) Metal matrix composites: materials, manufacturing and engineering. De Gruyter, Berlin
21. Mypati O, Panzer J, Robles-Linares J, Zan S, Liao Z, Axinte D (2024) Modelling and experimental study of laser-assisted milling of fibre reinforced SiC/Ti-6Al-4V metal matrix composite. Materials and Design 237. https://doi.org/10.1016/j.matdes.2023.112552
22. Kim J, Zani L, Abdul-Kadir A, Roy A, Baxevanakis K, Jones L, Silberschmidt V (2023) Hybrid-hybrid turning of micro-SiCp/AA2124 composites: a comparative study of laser-and-ultrasonic vibration-assisted machining. J Manuf Process 86:109–125. https://doi.org/10.1016/j.jmapro.2022.12.045

23. Marousi M, Rimpault X, Turenne S, Balazinski M (2023) Initial tool wear and process monitoring during titanium metal matrix composite machining (TiMMC). J Manuf Process 86:208–220. https://doi.org/10.1016/j.jmapro.2022.12.047
24. Bachchhav B (2021) Investigation on abrasive water jet machining of Al-Al2O3 MMC. Int J Indust Eng Prod Res 32:93–103. https://doi.org/10.22068/ijiepr.32.1.93
25. Marimuthu S, Dunleavey J, Liu Y, Antar M, Smith B (2019) Laser cutting of aluminium-alumina metal matrix composite. Opt Laser Technol 117:251–259. https://doi.org/10.1016/j.optlastec.2019.04.029
26. Rösiger A, Goller R, Langhof N, Krenkel W (2021) Influence of in-plane and out-of-plane machining on the surface topography, the removal mechanism and the flexural strength of 2D C/C-SiC composites. J Eur Ceram Soc 41:3108–3119. https://doi.org/10.1016/j.jeurceramsoc.2020.10.063
27. Chen J-P, Gu L, He G-J (2020) A review on conventional and nonconventional machining of SiC particle-reinforced aluminium matrix composites. Adv Manuf 8:279–315. https://doi.org/10.1007/s40436-020-00313-2
28. Hung N, Zhong Z, and Zhong C (1997) Grinding of metal matrix composites reinforced with silicon-carbide particles. Mater Manuf Process 12. https://doi.org/10.1080/10426919708935205
29. Du J, Zhou L, Li J, Yao Y (2014) Analysis of chip formation mechanism in mill-grinding of SiCp/Al composites. Mater Manuf Processes 29:1353–1360. https://doi.org/10.1080/10426914.2014.912309
30. Pai D, Rao S, Shetty R (2011) Application of statistical tool for optimisation of specific cutting energy and surface roughness on surface grinding of Al-SiC35p composites. Int J Sci Stat Comput 2:16–27
31. Thiagarajan C, Somasundaram S, Shankar P. Effect of grinding temperature during cylindrical grinding on surface finish of Al/SiC metal matrix composites
32. Kwak J, Kim Y (2008) Mechanical properties and grinding performance on aluminum-based metal matrix composites. J Mater Process Technol 201:596–600. https://doi.org/10.1016/j.jmatprotec.2007.11.139
33. Zhou L, Huang S, Yu X (2014) Machining characteristics in cryogenic grinding of SiCp/Al composites. Acta Metall. Sin. (Engl. Lett.) 27:869–874. https://doi.org/10.1007/s40195-014-0126-3
34. Zhao X, Gong Y, Liang G, Cai M, Han B (2021) Face grinding surface quality of high volume fraction SiCp/Al composite materials. Chin. J. Mech. Eng 34:34. https://doi.org/10.1186/s10033-020-00527-2
35. Roy S, Pal S, Ghosh S, Dey P (2008) Machining of interpenetrating phase alumina/aluminium composite by electrical discharge technique. Trans Indian Ceram Soc 67:75–80. https://doi.org/10.1080/0371750X.2008.11078644
36. Goswami R, Mitra S, Sarkar S (2009) Experimental investigation on electrochemical grinding (ECG) of alumina-aluminum interpenetrating phase composite. Int J Adv Manuf Technol 40:729–741. https://doi.org/10.1007/s00170-008-1382-z
37. Liu J, Wu J, Binner J (2017) Cutting resistance of metal-ceramic interpenetrating composites. Ceram Int 43:2815–2823. https://doi.org/10.1016/j.ceramint.2016.11.124
38. Rösiger A (2022) Einfluss der Schleif- und Fräsbearbeitung auf die Oberflächenqualität und die mechanischen Eigenschaften von kohlenstofffaserverstärktem Siliziumcarbid, 1st edn. Cuvillier Verlag, Göttingen
39. Karabulut Ş, Çinici H, Karakoç H (2016) Experimental investigation and optimization of cutting force and tool wear in milling Al7075 and open-cell SiC foam composite. Arab J Sci Eng 41:1797–1812. https://doi.org/10.1007/s13369-015-1991-4
40. Karabulut Ş, Karakoç H (2017) Investigation of surface roughness in the milling of Al7075 and open-cell SiC foam composite and optimization of machining parameters. Neural Comput & Applic 28:313–327. https://doi.org/10.1007/s00521-015-2058-x
41. Da Silva LF (ed) (2017) Materials design and applications. Springer International Publishing, Cham, Switzerland
42. Hikmat M, Rostam S, Ahmed Y (2021) Investigation of tensile property-based Taguchi method of PLA parts fabricated by FDM 3D printing technology. Results Eng 11:100264. https://doi.org/10.1016/j.rineng.2021.100264
43. Liu X, Zhang M, Li S, Si L, Peng J, Hu Y (2017) Mechanical property parametric appraisal of fused deposition modeling parts based on the gray Taguchi method. Int J Adv Manuf Technol 89:2387–2397. https://doi.org/10.1007/s00170-016-9263-3
44. Kahraman M, Öztürk S (2019) Experimental study of newly structural design grinding wheel considering response surface optimization and Monte Carlo simulation. Measurement 147. https://doi.org/10.1016/j.measurement.2019.07.053
45. Öztürk S, Kahraman M (2019) Modeling and optimization of machining parameters during grinding of flat glass using response surface methodology and probabilistic uncertainty analysis based on Monte Carlo simulation. Measurement 145:274–291. https://doi.org/10.1016/j.measurement.2019.05.098
46. Schukraft J, Lohr C, Weidenmann KA (2020) Mechanical characterization of an interpenetrating metal-matrix composite based on highly homogeneous ceramic foams. In: Hausmann JM, Siebert M, von Hehl A, Weidenmann KA (eds) 4th International Conference Hybrid - Materials and Structures. Sankt Augustin
47. Horny D, Schukraft J, Pieper C, Weidenmann K, Schulz K (2023) Numerical and experimental investigation on the self-healing potential of interpenetrating metal-ceramic composites. Adv Eng Mater. https://doi.org/10.1002/adem.202300259
48. Klocke F (2018) Fertigungsverfahren 2. Springer Berlin Heidelberg, Berlin, Heidelberg
49. Uhlmann EG (1994) Tiefschleifen hochfester keramischer Werkstoffe Carl Hanser Verlag. München
50. Huang G, Yu K, Zhang M, Guo H, Xu X (2018) Grinding characteristics of aluminium alloy 4032 with a brazed diamond wheel. Int J Adv Manuf Technol 95:4573–4581. https://doi.org/10.1007/s00170-017-1540-2
51. Anand Ronald B, Vijayaraghavan L, Krishnamurthy R (2009) Studies on the influence of grinding wheel bond material on the grindability of metal matrix composites. Mater Des 30:679–686. https://doi.org/10.1016/j.matdes.2008.05.038
52. Li Z, Ding W, Shen L, Xi X, Fu Y (2016) Comparative investigation on high-speed grinding of TiCp/Ti–6Al–4V particulate reinforced titanium matrix composites with single-layer electroplated and brazed CBN wheels. Chin J Aeronaut 29:1414–1424. https://doi.org/10.1016/j.cja.2016.01.005
53. Liu C, Ding W, Yu T, Yang C (2018) Materials removal mechanism in high-speed grinding of particulate reinforced titanium matrix composites. Precis Eng 51:68–77. https://doi.org/10.1016/j.precisioneng.2017.07.012
54. Malkin S (2008) Grinding technology: theory and applications of machining with abrasives, 2nd edn. Industrial Press, New York, NY
55. Werner G (1971) Kinematik und Mechanik des Schleifprozesses Doktorarbeit Rheinisch-Westfälischen Technischen Hochschule Aachen
56. Paucksch E, Linß M (2008) Zerspantechnik: Prozesse, Werkzeuge, Technologien, 12th edn. Vieweg + Teubner, Wiesbaden
57. Spur G (1989) Keramikbearbeitung - Schleifen, Honen, Läppen. Hanser, Abtragen
58. Zan S, Liao Z, Robles-Linares J, Garcia Luna G, Axinte D (2023) Machining of long ceramic fibre reinforced metal matrix composites – how could temperature influence the cutting mechanisms? International Journal of Machine Tools and Manufacture 185. https://doi.org/10.1016/j.ijmachtools.2023.103994